

Supersymmetric Higgs production in gluon fusion at next-to-leading order

Robert V. Harlander

*Institut für Theoretische Teilchenphysik, Universität Karlsruhe
D-76128 Karlsruhe, Germany
E-mail: robert.harlander@cern.ch*

Matthias Steinhauser

*II. Institut für Theoretische Physik, Universität Hamburg
D-22761 Hamburg, Germany
E-mail: matthias.steinhauser@desy.de*

ABSTRACT: The next-to-leading order (NLO) QCD corrections to the production and decay rate of a Higgs boson are computed within the framework of the Minimal Supersymmetric Standard Model (MSSM). The calculation is based on an effective theory for light and intermediate mass Higgs bosons. We provide a `Fortran` routine for the numerical evaluation of the coefficient function. For most of the MSSM parameter space, the relative size of the NLO corrections is typically of the order of 5% smaller than the Standard Model value. We exemplify the numerical results for two scenarios: the benchmark point SPS 1a, and a parameter region where the gluon-Higgs coupling at leading order is very small due to a cancellation of the squark and quark contributions.

Contents

1. Introduction	1
2. Effective Lagrangian through next-to-leading order	3
2.1 Effective Lagrangian	3
2.2 Leading order coefficient function	5
2.3 Next-to-leading order coefficient function	6
3. Results	7
3.1 Results for C_1	7
3.2 Hadronic decay rate	11
3.3 Hadronic production rate	12
3.4 Discussion	16
4. Conclusions	16
A. Feynman rules	18
A.1 Definitions	18
A.2 Feynman rules used in this calculation	19
B. Renormalization and decoupling constants	21
C. Description of evalcsusy.f	24

1. Introduction

The most important Higgs production cross sections at the Tevatron and the Large Hadron Collider (LHC) are known quite reliably within the Standard Model framework. Weak boson fusion as well as associated production of Higgs bosons with a top quark pair are known with NLO QCD accuracy (see Refs. [1, 2] and [3–5], respectively), while gluon fusion and Higgs-Strahlung are even known through NNLO in QCD (see Refs. [6–15] and Ref. [16]).

At this level of accuracy, also electro-weak corrections can be important. They have been evaluated to first order for the Higgs-Strahlung process [17] (a combined analysis of QCD and electro-weak effects can be found in [18]). For the gluon fusion process, only very recently the full set of first order electro-weak effects has been completed (for $M_h < 2M_W$): The contribution from light fermion loops at two-loop order was evaluated in Ref. [19], the top quark induced effects were calculated in Ref. [20]. The terms of order $G_F m_t^2$ have been known for ten years [21], and additional QCD effects of order $\alpha_s G_F m_t^2$ can be extracted from the result of Ref. [22].

One remarkable fact about the gluon fusion process is that it has no tree-level contribution. It is therefore sensitive to new particles that can mediate the gluon-Higgs coupling. In the Standard Model, this coupling is dominated by a top quark loop, with a small contribution also from bottom quarks. In the MSSM, the bottom quark contribution can be enhanced for large values of $\tan\beta$. Their NLO effects have been evaluated in Refs. [8, 9].

In this paper, we consider the gluon-Higgs coupling mediated by quarks and squarks at NLO and its effects on the hadronic production and decay of a light or intermediated mass scalar Higgs boson. A preliminary study of these effects has been published in Ref. [23], where, however, only a very restricted parameter range of the MSSM has been used. In particular, mixing in the stop sector was neglected. In this work we dismiss these constraints. In combination with Refs. [8, 9] for the bottom loops, we thus provide the NLO result for almost all of the SUSY parameter space. The only restrictions are in the region where sbottom-effects become important. However, this only happens when the sbottom mixing angle is $\theta_b \approx 45^\circ$ and both the mass splitting between \tilde{b}_1 and \tilde{b}_2 as well as $\tan\beta$ are very large.

The outline of the paper is as follows. In Sect. 2, we construct the effective Lagrangian for the gluon-Higgs interaction by integrating out the top quark as well as all supersymmetric particles of the MSSM. The Lagrangian at leading order in $1/M$ ($M \in \{m_t, m_{\tilde{t}}, m_{\tilde{g}}\}$) contains only one operator. We evaluate its universal Wilson coefficient through NLO. In Sect. 3, we first study the behavior of the NLO Wilson coefficient itself, and subsequently use it to evaluate the hadronic decay and production rate of the light, CP-even Higgs boson of the MSSM. To this aim, we choose two specific sets of SUSY parameters: The first one is the benchmark SPS 1a, defined in Ref. [24]. The second one is similar to the “gluophobic Higgs” scenario of Ref. [25], where the squark and the quark contributions to the gluon-Higgs coupling nearly cancel each other [26]. In Sect. 4, we present our conclusions. App. A and B collect the Feynman rules, counter terms, and decoupling constants that we used in our calculation. App. C describes the **Fortran** routine that we provide to evaluate the first and second order Wilson coefficient.

2. Effective Lagrangian through next-to-leading order

2.1 Effective Lagrangian

The effective Lagrangian is constructed from the full MSSM Lagrangian by integrating out all SUSY partners and the top quark. The field content of the effective theory is thus the same as when starting from the Standard Model Lagrangian. Therefore, also the effective Lagrangian has the same form. It is given by

$$\mathcal{L}_{\text{eff}} = -\frac{h}{v} C_1^{\text{B}} \mathcal{O}_1^{\text{B}}, \quad \mathcal{O}_1^{\text{B}} = \frac{1}{4} G_{a,\mu\nu}^{\text{B}} G_a^{\text{B},\mu\nu}, \quad (2.1)$$

where $G_{a,\mu\nu}^{\text{B}}$ is the bare gluonic field strength tensor, $v \approx 246 \text{ GeV}$, and C_1^{B} is the matching coefficient to the full theory. For the sake of simplicity of the discussion, we focus on the light neutral Higgs, denoted h , in this paper. The translation of the formulas to the heavy neutral Higgs is straightforward, but the validity of the effective theory approach of Eq. (2.1) has to be carefully checked in this case.

For the Standard Model, the two-loop α_s^2 corrections for $C_1(\alpha_s)$ have been calculated in Ref. [6, 7], the α_s^3 and α_s^4 terms in Ref. [27, 28] and Ref. [29], respectively. Furthermore, as mentioned in the introduction, electroweak corrections of order $G_{\text{F}} m_t^2$ and $\alpha_s G_{\text{F}} m_t^2$ have been evaluated Refs. [21] and [22], respectively. For the MSSM, the two-loop QCD corrections are known in the case of zero squark mixing [23].

The QCD renormalization of C_1^{B} and \mathcal{O}_1^{B} is discussed in Refs. [29, 30] and is given by

$$C_1 = Z_{11}^{-1} C_1^{\text{B}}, \quad \mathcal{O}_1 = Z_{11} \mathcal{O}_1^{\text{B}}, \quad \text{with} \quad Z_{11} = \left(1 - \frac{\pi \beta}{\alpha_s \epsilon}\right)^{-1}, \quad (2.2)$$

where

$$\beta(\alpha_s) = -\left(\frac{\alpha_s}{\pi}\right)^2 \beta_0 + \mathcal{O}(\alpha_s^3) \quad (2.3)$$

is the β -function of standard ($n_l = 5$)-flavor QCD, with $\beta_0 = 11/4 - n_l/6$. Note that here and in what follows, α_s denotes the strong coupling constant in standard five-flavor QCD; it is a function of the renormalization scale μ_{R} :

$$\alpha_s \equiv \alpha_s^{(5)}(\mu_{\text{R}}). \quad (2.4)$$

In this paper we calculate C_1 in the MSSM through α_s^2 , i.e., we will evaluate the coefficients $c_1^{(0)}$ and $c_1^{(1)}$ defined as

$$C_1 = -\frac{\alpha_s}{3\pi} \left[c_1^{(0)} + \frac{\alpha_s}{\pi} c_1^{(1)} + \mathcal{O}(\alpha_s^2) \right]. \quad (2.5)$$

This will allow us to compute the NLO approximation to the hadronic production and decay rate of a CP-even Higgs boson. Following the argumentation of Ref. [31], we can even derive a fairly accurate estimate of the NNLO production cross section in this model.

Several methods to compute the coefficient function C_1 are described in Ref. [32]. Here we follow the most direct one which is based on the relation

$$\zeta_3^B C_1^B = -\frac{1}{4} \left(\frac{g^{\mu\nu}(p_1 \cdot p_2) - p_1^\nu p_2^\mu - p_1^\mu p_2^\nu}{(D-2)(p_1 \cdot p_2)^2} \Gamma_{\mu\nu}^B(p_1, p_2) \right) \Big|_{p_1=p_2=0}. \quad (2.6)$$

$\Gamma_{\mu\nu}^B(p_1, p_2)$ is the 1-particle-irreducible vertex function of two gluons in a color-singlet state (incoming momenta p_1, p_2) and a Higgs boson in the full theory. ζ_3^B is the decoupling constant that relates the gluon field in the full and the effective theory (details can be found in Ref. [32]). It can be computed from the gluon propagator in the full theory $\Pi_g^B(p)$ through

$$\zeta_3^B = 1 + \Pi_g^B(p=0). \quad (2.7)$$

The result for ζ_3^B is given in Eq. (B.10).

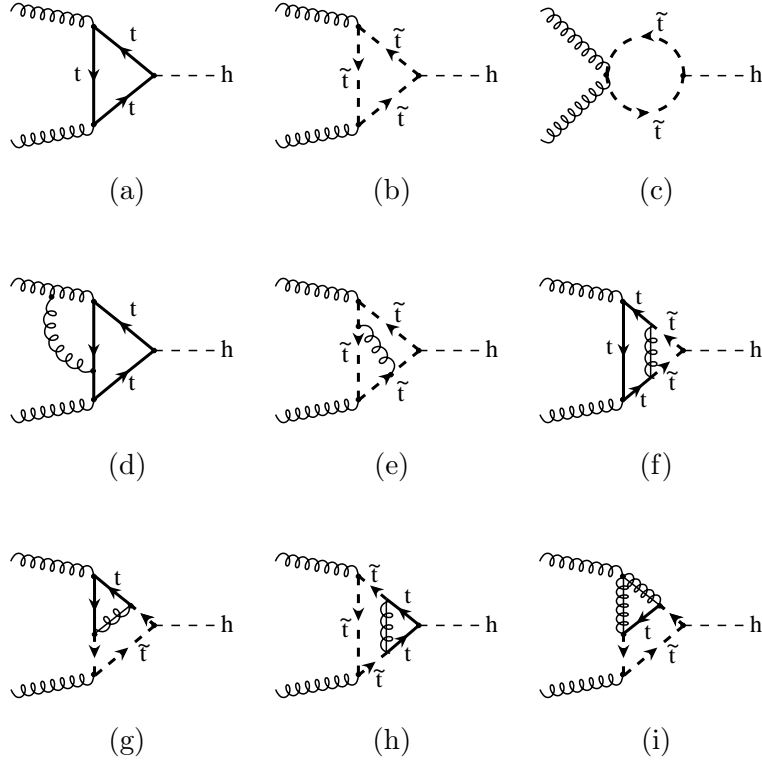


Figure 1: Diagrams contributing to the effective ggh coupling in the MSSM.

Sample diagrams corresponding to $\Gamma_{\mu\nu}^B$ are shown in Fig. 1. We may distinguish three different types:

1. pure top contributions, e.g. Fig. 1 (a) and (d)
2. pure stop contributions, e.g. Fig. 1 (b), (c), and (e)
3. mixed top/stop/gluino contributions, e.g. Fig. 1 (f)-(i)

The pure top quark contributions are separately finite (they correspond to the Standard Model terms), while the pure stop and the mixed contributions each develop ultra-violet poles that cancel in their sum (after taking into account the proper counter terms). Application of Eq. (2.6) leads to one- and two-loop integrals with vanishing external momenta. They can be evaluated in closed form using the algorithm of Davydychev and Tausk [33]. Details will be given in Sect. 2.3.

2.2 Leading order coefficient function

The LO approximation of the coefficient function is obtained from the one-loop diagrams of Fig. 1 (a), (b), and (c). The result is

$$\begin{aligned}
c_1^{(0)} &= c_{1,t}^{(0)} + c_{1,\tilde{t}}^{(0)}, & c_{1,t}^{(0)} &= \frac{\cos \alpha}{\sin \beta}, \\
c_{1,\tilde{t}}^{(0)} &= \frac{\cos \alpha}{\sin \beta} \left[\frac{1}{4} \left(\frac{m_t^2}{m_{\tilde{t}_1}^2} + \frac{m_t^2}{m_{\tilde{t}_2}^2} \right) + \frac{\sin^2 2\theta_t}{8} \left(1 - \frac{m_{\tilde{t}_1}^2}{2m_{\tilde{t}_2}^2} - \frac{m_{\tilde{t}_2}^2}{2m_{\tilde{t}_1}^2} \right) \right] \\
&+ \frac{1}{8} \mu_{\text{SUSY}} m_t \frac{\cos(\alpha - \beta)}{\sin^2 \beta} \sin 2\theta_t \left[\frac{1}{m_{\tilde{t}_1}^2} - \frac{1}{m_{\tilde{t}_2}^2} \right] \\
&+ \frac{c_1^{\text{EW}} + c_2^{\text{EW}}}{16} \left(\frac{m_t^2}{m_{\tilde{t}_1}^2} + \frac{m_t^2}{m_{\tilde{t}_2}^2} \right) + \frac{c_1^{\text{EW}} - c_2^{\text{EW}}}{16} \cos 2\theta_t \left(\frac{m_t^2}{m_{\tilde{t}_1}^2} - \frac{m_t^2}{m_{\tilde{t}_2}^2} \right).
\end{aligned} \tag{2.8}$$

Here and in the following we assume all masses in the on-shell scheme, if not stated otherwise (m_t , $m_{\tilde{t}_i}$, and $m_{\tilde{g}}$ are the top, stop ($i = 1, 2$) and gluino mass, respectively). α is the mixing angle between the weak and the mass eigenstates of the neutral scalar Higgs bosons, $\tan \beta$ is the ratio of the vacuum expectation values of the two Higgs doublets, μ_{SUSY} is the coefficient of the bilinear Higgs term in the MSSM superpotential, c_1^{EW} and c_2^{EW} are defined in Eq. (A.7), and the mixing angle θ_t between the helicity (\tilde{t}_L, \tilde{t}_R) and mass eigenstates (\tilde{t}_1, \tilde{t}_2) of the top squarks is defined in Sect. A.1. For more details on the MSSM parameters, see Ref. [34], for example. $c_{1,t}^{(0)}$ and $c_{1,\tilde{t}}^{(0)}$ are the top- and stop-loop contributions, respectively. Note that the latter are not necessarily suppressed for large stop masses. In fact, due to the term $\propto \sin^2 2\theta_t$, they can be dominant for large stop mixing and large mass splitting between \tilde{t}_1 and \tilde{t}_2 [26]. Using Eq. (A.2), this term can be written as

$$\frac{\sin^2 2\theta_t}{8} \left(1 - \frac{m_{\tilde{t}_1}^2}{2m_{\tilde{t}_2}^2} - \frac{m_{\tilde{t}_2}^2}{2m_{\tilde{t}_1}^2} \right) = -X_t^2 \frac{m_t^2}{4m_{\tilde{t}_1}^2 m_{\tilde{t}_2}^2}, \tag{2.9}$$

implying that the squark effects are large when $X_t = A_t - \mu_{\text{SUSY}} \cot \beta$ is large. In addition, Eq. (2.8) shows that large effects can also arise from large values of μ_{SUSY} .

The question arises if cancellations between the quark and squark contributions occur also when radiative corrections are included, or if the regions where this occurs are significantly different from the LO prediction. We will discuss this issue for a specific example in Sect. 3.

2.3 Next-to-leading order coefficient function

A major difference between the Standard Model and the SUSY calculation for C_1 is the occurrence of more than one mass scale in SUSY; this leads to expressions for C_1 that are much more complicated and unhandy as compared to the Standard Model result. The latter depends only on the top quark mass and thus involves only constants and logarithms of the form $\ln(\mu_R^2/m_t^2)$, where μ_R is the renormalization scale. In fact, let us recall the expression in the Standard Model [27, 28]:

$$C_1^{\text{SM}} = -\frac{\alpha_s}{3\pi} \left\{ 1 + \frac{11}{4} \frac{\alpha_s}{\pi} + \left[\frac{2777}{288} + \frac{19}{16} \ln \frac{\mu_R^2}{m_t^2} - n_l \left(\frac{67}{96} - \frac{1}{3} \ln \frac{\mu_R^2}{m_t^2} \right) \right] \left(\frac{\alpha_s}{\pi} \right)^2 \right\} + \mathcal{O}(\alpha_s^4), \quad (2.10)$$

where for convenience we also displayed the NNLO result.

The calculation of $c_1^{(1)}$ in the MSSM leads to two-loop integrals with up to three different masses $m_1, m_2, m_3 \in \{m_t, m_{\tilde{t}_1}, m_{\tilde{t}_2}, m_{\tilde{g}}\}$ (integrals with four different masses can be transformed to integrals with three different masses by simple partial fractioning). Davydychev and Tausk have provided an algorithm for their analytic evaluation [33]. It allows one to express the integrals through the function

$$\tilde{\Phi}(m_1, m_2, m_3) = (m_3 \lambda)^2 \begin{cases} \Phi_1 \left(\frac{m_1^2}{m_3^2}, \frac{m_2^2}{m_3^2} \right), & m_1 + m_2 \leq m_3, \\ \Phi_2 \left(\frac{m_1^2}{m_3^2}, \frac{m_2^2}{m_3^2} \right), & m_1 + m_2 > m_3, \end{cases} \quad (2.11)$$

where

$$\Phi_1(x, y) = \frac{1}{\lambda} \left\{ 2 \ln \left[\frac{1}{2} (1 + x - y - \lambda) \right] \ln \left[\frac{1}{2} (1 - x + y - \lambda) \right] - \ln x \ln y - 2 \text{Li}_2 \left[\frac{1}{2} (1 + x - y - \lambda) \right] - 2 \text{Li}_2 \left[\frac{1}{2} (1 - x + y - \lambda) \right] + \frac{1}{3} \pi^2 \right\}, \quad (2.12)$$

and

$$\Phi_2(x, y) = \frac{2}{\sqrt{-\lambda^2}} \left\{ \text{Cl}_2 \left[2 \arccos \left(\frac{-1 + x + y}{2\sqrt{xy}} \right) \right] + \text{Cl}_2 \left[2 \arccos \left(\frac{1 + x - y}{2\sqrt{x}} \right) \right] + \text{Cl}_2 \left[2 \arccos \left(\frac{1 - x + y}{2\sqrt{y}} \right) \right] \right\}, \quad (2.13)$$

$$\lambda = \sqrt{(1 - x - y)^2 - 4xy}, \quad x = \frac{m_1^2}{m_3^2}, \quad y = \frac{m_2^2}{m_3^2}. \quad (2.14)$$

$\text{Li}_2(x)$ is the standard dilogarithm and $\text{Cl}_2(x)$ is Clausen's integral function,

$$\text{Li}_2(x) = -\int_0^1 dt \frac{\ln(1 - xt)}{t}, \quad \text{Cl}_2(x) = -\int_0^x dt \ln |2 \sin(t/2)|. \quad (2.15)$$

Note that $\tilde{\Phi}(m_1, m_2, m_3)$ is symmetric in m_1, m_2 and m_3 .

To regulate the ultra-violet divergences of the loop integrals, we use Dimensional Reduction (DRED). This is realized by evaluating all Dirac traces and Lorentz contractions in four,

and all loop integrals in $d = (4 - 2\epsilon)$ space-time dimensions [35,36]. The external projector defined in Eq.(2.6) is taken in d dimensions. Renormalization is done as explained in App.B.

Note that even though we only keep the top- and stop-Higgs couplings different from zero, squarks of other flavors (\tilde{b} , \tilde{c} etc.) may enter the NLO calculation through the four-squark vertex listed in App.A.2. Typical diagrams are shown in Fig.2. However, diagrams like Fig.2 (a) vanish due to their color factor, and the diagrams like the one in Fig.2 (b) add up to zero.

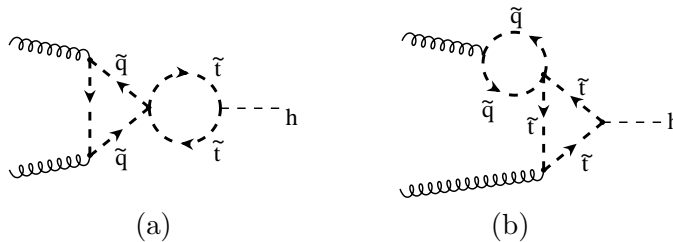


Figure 2: Diagrams involving \tilde{q} , with $q \in \{u, d, c, s, t, b\}$.

The full result for $c_1^{(1)}$ in the MSSM is too long to be quoted here.¹ Instead, we provide a Fortran code, named `evalcsusy.f` [38], that allows for a numerical evaluation of the coefficient function and can be combined with other programs quite easily using an SLHA-like interface (SLHA: SUSY Les Houches Accord [39]). For details, see App. C.

As a check of our result, we also calculated the diagrams by means of asymptotic expansions, using the program EXP [40]. It allows us to evaluate an approximate result for C_1 , provided that there is a certain hierarchy among the masses $m_t, m_{\tilde{t}_1}, m_{\tilde{t}_2}$, and $m_{\tilde{q}}$. The approximation, however, will only be valid within the radius of convergence of the specific series, so that we will not make use of it in our phenomenological analyses below. Needless to say that the expansion of the analytic result expressed through Eq. (2.11) agrees with the corresponding result obtained through asymptotic expansions.

As another check, we reproduced the results of an earlier publication of ours [23] which was obtained by asymptotic expansions and in a very simplifying limit.

3. Results

3.1 Results for C_1

In order to get an impression about the typical size of the corrections we consider two scenarios. First, we look at the behavior of $c_1^{(0)}$ and $c_1^{(1)}$ at and along a ‘‘Snowmass Point and Slope’’ (SPS) [24]. In the second case we consider a particular region of the parameter space where C_1 shows large deviations from its Standard Model value.

¹All algebraic manipulations were done with the help of FORM [37].

To be specific, let us assume an mSUGRA scenario² with the five parameters m_0 , $m_{1/2}$, A_0 , $\tan\beta$, and $\text{sign}(\mu_{\text{SUSY}})$. In addition, we define the following Standard Model parameters:

$$\begin{aligned} M_Z &= 91.1876 \text{ GeV}, & \bar{m}_b &= 4.2 \text{ GeV}, & m_t &= 178 \text{ GeV}, & m_\tau &= 1.777 \text{ GeV}, \\ \alpha_{\text{QED}}^{-1}(M_Z) &= 127.934, & G_F &= 1.16637 \cdot 10^{-5} \text{ GeV}^{-2}, & \alpha_s(M_Z) &= 0.118, \end{aligned} \quad (3.1)$$

where M_Z is the Z boson mass, $\bar{m}_b \equiv \bar{m}_b(\bar{m}_b)$ is the scale-invariant $\overline{\text{MS}}$ value of the bottom quark mass, m_t is the pole mass of the top quark and m_τ is the mass of the τ lepton. $\alpha_{\text{QED}}(M_Z)$ is the running electromagnetic coupling at M_Z , G_F is the Fermi constant and α_s the strong coupling. As discussed in App. B, we further need to define the (arbitrary) scale q_0 (see Eq. (B.7)) that enters the renormalization constant of the stop mixing angle θ_t , as well as the usual renormalization scale μ_R . As our default values we adopt

$$q_0 = \frac{1}{2} (m_{\tilde{t}_1} + m_{\tilde{t}_2}), \quad \mu_R = M_h. \quad (3.2)$$

M_h is the mass of the light CP-even Higgs boson. Both of these choices are generally considered to be typical values which avoid the explicit occurrence of large logarithmic corrections.

As already mentioned above and explained in detail in App. C, the input and output files of the program `evalcsusy.f` follow the SLHA conventions [39]. Among the various SUSY-spectrum calculators which are currently available [41–44] (see, e.g., Ref. [45] for a comparison), only `SoftSusy` [42] and `SPheno` [44] support the SLHA conventions for both in- and output. Therefore, we will use these two generators in our analysis. For our applications they provide almost identical results.

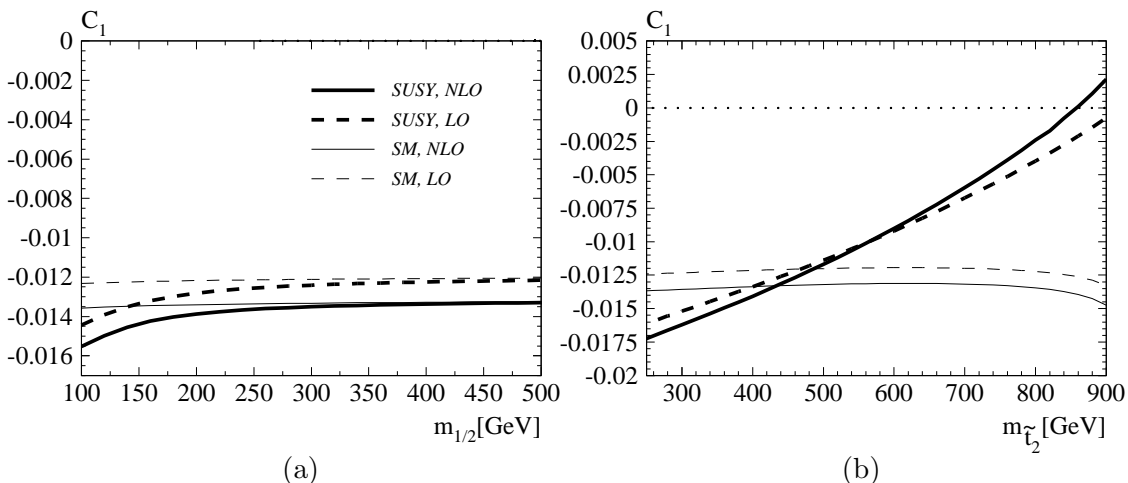


Figure 3: LO (dashed) and NLO (solid) result for C_1 : (a) as a function of $m_{1/2}$ for the SPS 1a scenario; (b) as a function of $m_{\tilde{t}_2}$ for the scenario defined in Eq. (3.8). The other parameters are fixed as described in the main text. The corresponding Standard Model results are shown as thin lines.

²Typical GMSB and AMSB scenarios as defined by SPS 7 and SPS 9 [24] give qualitatively similar results.

SPS 1a is defined through the following input parameters:

$$\begin{aligned}
m_0 &= 100 \text{ GeV}, \\
m_{1/2} &= 250 \text{ GeV}, \\
A_0 &= -100 \text{ GeV}, \\
\tan \beta &= 10, \\
\text{sign}(\mu_{\text{SUSY}}) &= +1.
\end{aligned}
\tag{3.3}$$

Using `SoftSusy` or `SPheno` to derive the low energy parameters that enter our result and passing them to `evalcsusy.f` as input, one finds

$$c_1^{(0)} \approx 1.03, \quad c_1^{(1)} \approx 2.44, \tag{3.4}$$

which is close to the Standard Model values

$$c_1^{(0)} = 1, \quad c_1^{(1)} = \frac{11}{4} = 2.75. \tag{3.5}$$

The slope corresponding to SPS 1a is given by

$$m_0 = -A_0 = 0.4 m_{1/2}, \quad m_{1/2} \text{ varies}. \tag{3.6}$$

The dependence of C_1 along this slope is shown as thick lines in Fig. 3 (a) at LO (dashed) and NLO (solid). One observes a moderate increase in magnitude of about 8% when going from LO to NLO. The thin lines correspond to the Standard Model results. The small variation of the latter is due to their dependence on M_h through $\alpha_s(M_h)$. For completeness, let us remark that the masses that enter our calculation change monotonously within the following ranges when going from $m_{1/2} = 100 \text{ GeV}$ to $m_{1/2} = 500 \text{ GeV}$:

$$\begin{aligned}
101 \text{ GeV} &\leq M_h \leq 118 \text{ GeV}, \\
176 \text{ GeV} &\leq m_{\tilde{t}_1} \leq 784 \text{ GeV}, \\
330 \text{ GeV} &\leq m_{\tilde{t}_2} \leq 1019 \text{ GeV}, \\
268 \text{ GeV} &\leq m_{\tilde{g}} \leq 1158 \text{ GeV}.
\end{aligned}
\tag{3.7}$$

The dependence of $m_{\tilde{t}_1}$, $m_{\tilde{t}_2}$, and $m_{\tilde{g}}$ on $m_{1/2}$ is almost linear. The dependence of M_h on $m_{1/2}$ is shown in Fig. 4 (a).

In a second example, we consider a case where the LO squark and quark contributions to the gluon-Higgs coupling largely cancel each other [26]. Thus, we do not refer to any SUSY breaking scenario, but directly choose the following low energy parameters:³

$$\begin{aligned}
m_t &= 178 \text{ GeV}, \quad m_{\tilde{t}_1} = 200 \text{ GeV}, \quad m_{\tilde{g}} = 1000 \text{ GeV}, \quad M_W = 80.425 \text{ GeV}, \\
\tan \beta &= 10, \quad \alpha = 0, \quad \theta_t = \frac{\pi}{4}, \quad 250 \text{ GeV} \leq m_{\tilde{t}_2} \leq 900 \text{ GeV}.
\end{aligned}
\tag{3.8}$$

³A qualitatively similar benchmark point (“gluophobic Higgs”) has been suggested in Ref. [46].

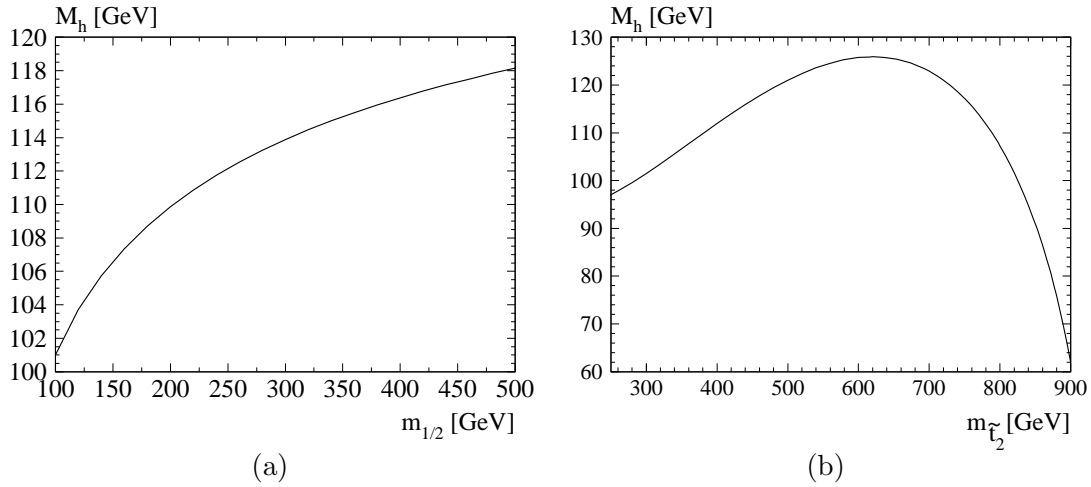


Figure 4: M_h as a function of (a) $m_{1/2}$ along the slope of SPS 1a, and (b) $m_{\tilde{t}_2}$ for the scenario defined in Eq. (3.8).

The light Higgs boson mass is determined by the approximate two-loop formula [47]

$$M_h^2 = M_Z^2 + M_{h,\alpha}^2 + M_{h,\alpha\alpha_s}^2, \quad (3.9)$$

with

$$M_{h,\alpha}^2 = \frac{3 G_F \sqrt{2}}{2 \pi^2} \left\{ -\ln \left(\frac{m_t^2}{M_S^2} \right) + \frac{X_t^2}{M_S^2} \left(1 - \frac{1}{12} \frac{X_t^2}{M_S^2} \right) \right\},$$

$$M_{h,\alpha\alpha_s}^2 = -3 \frac{G_F \sqrt{2}}{\pi^2} \frac{\alpha_s}{\pi} m_t^4 \left\{ \ln^2 \left(\frac{m_t^2}{M_S^2} \right) - \left(2 + \frac{X_t^2}{M_S^2} \right) \ln \left(\frac{m_t^2}{M_S^2} \right) - \frac{X_t}{M_S} \left(2 - \frac{1}{4} \frac{X_t^3}{M_S^3} \right) \right\}. \quad (3.10)$$

In this approximation and for $\theta_t = \pi/4$, the parameters X_t and M_S are related to the stop masses through

$$X_t = \frac{1}{2m_t} \left(m_{\tilde{t}_1}^2 - m_{\tilde{t}_2}^2 \right), \quad M_S^2 = \frac{1}{2} \left(m_{\tilde{t}_1}^2 + m_{\tilde{t}_2}^2 \right). \quad (3.11)$$

The variation of M_h within the parameter range of Eq. (3.8) is shown in Fig. 4 (b).

The choice of θ_t is motivated by the explicit result for $c_1^{(0)}$ in Eq. (2.8) (see also Eq. (2.9)), where the prefactor of the last term in the first line becomes maximal for $\theta_t = \pi/4$. The expression in brackets vanishes for $m_{\tilde{t}_1} = m_{\tilde{t}_2}$. However, in the limit $m_{\tilde{t}_1} \ll m_{\tilde{t}_2}$ a term enhanced by $m_{\tilde{t}_2}^2/m_{\tilde{t}_1}^2$ survives which can dominate the result for $c_1^{(0)}$. This is shown in Fig. 3 (b) where C_1 and C_1^{SM} are plotted as a function of $m_{\tilde{t}_2}$. One observes a rather strong variation of the one-loop result of C_1 . It even changes sign close to $m_{\tilde{t}_2} \approx 900$ GeV, where the SUSY and the Standard Model contributions cancel each other. A similar behavior is observed at NLO, where C_1 vanishes for $m_{\tilde{t}_2} \approx 850$ GeV.

3.2 Hadronic decay rate

For our numerical analysis we neglect all bottom and sbottom effects. In particular, the direct coupling of a Higgs boson to bottom quarks is not contained in our formulae. In this approximation the LO result for the hadronic decay of a light Higgs boson is determined through the $h \rightarrow gg$ amplitude shown in Fig. 1 (a)–(c). At higher orders, also multi-particle final states contribute, such as ggg , $gq\bar{q}$, $ggq\bar{q}$, etc. ($q \neq t$). We write

$$\Gamma(h \rightarrow \text{hadrons}) \equiv \Gamma_g^h = F_0 \cdot \left(\frac{C_1}{c_1^{(0)}} \right)^2 (1 + \delta_{\text{PS}}) = F_0 \cdot \left(\frac{\alpha_s}{3\pi} \right)^2 (1 + \delta), \quad (3.12)$$

with

$$F_0 = \frac{M_h^3 \sqrt{2} G_{\text{F}}}{8\pi} \left| g_t^h A(\tau_t) + \frac{m_t^2}{2m_{\tilde{t}_1}^2} g_{t,11}^h \tilde{A}(\tau_1) + \frac{m_t^2}{2m_{\tilde{t}_2}^2} g_{t,22}^h \tilde{A}(\tau_2) \right|^2, \quad (3.13)$$

$$\tau_t = \frac{4m_t^2}{M_h^2}, \quad \tau_i = \frac{4m_{\tilde{t}_i}^2}{M_h^2}, \quad i = 1, 2.$$

The second equality in Eq. (3.12) illustrates our approach: the exact leading order result proportional to F_0 is factored out, and the corrections are treated in the effective-theory approach of Eq. (2.1). The quantity δ_{PS} contains the real and virtual corrections associated with the operator \mathcal{O}_1 . The third equality in Eq. (3.12) is obtained by expanding the ratio $C_1/c_1^{(0)}$ in terms of α_s . The coupling constants g_t^h and $g_{t,ij}^h$ in Eq. (3.13) are defined in Eqs. (A.4)–(A.6), and

$$A(t) = \frac{3}{2} t [1 + (1-t)f(t)], \quad \tilde{A}(t) = -\frac{3}{4} t [1 - t f(t)], \quad (3.14)$$

where

$$f(t) = \begin{cases} \arcsin^2\left(\frac{1}{\sqrt{t}}\right), & t \geq 1, \\ -\frac{1}{4} \left[\ln \frac{1+\sqrt{1-t}}{1-\sqrt{1-t}} - i\pi \right]^2, & t < 1. \end{cases} \quad (3.15)$$

For completeness, we remark that the limits for $t \rightarrow \infty$ are given by

$$\lim_{t \rightarrow \infty} A(t) = 1, \quad \lim_{t \rightarrow \infty} \tilde{A}(t) = \frac{1}{4}, \quad (3.16)$$

and thus,

$$F_0 \rightarrow \frac{M_h^3 \sqrt{2} G_{\text{F}}}{8\pi} |c_1^{(0)}|^2 \quad \text{for } m_t, m_{\tilde{t}}, m_{\tilde{g}} \gg M_h, \quad (3.17)$$

where $c_1^{(0)}$ is given in Eq. (2.8). The quantity δ is expanded in terms of α_s as follows:

$$\delta = \frac{\alpha_s}{\pi} \delta^{(1)} + \left(\frac{\alpha_s}{\pi} \right)^2 \delta^{(2)} + \mathcal{O}(\alpha_s^3), \quad (3.18)$$

and similarly for δ_{PS} . The relation between δ_{PS} and δ is given by

$$\delta^{(1)} = \delta_{\text{PS}}^{(1)} + 2\frac{c_1^{(1)}}{c_1^{(0)}}, \quad \delta^{(2)} = \delta_{\text{PS}}^{(2)} + 2\frac{c_1^{(1)}}{c_1^{(0)}}\delta_{\text{PS}}^{(1)} + 2\frac{c_1^{(2)}}{c_1^{(0)}} + \left(\frac{c_1^{(1)}}{c_1^{(0)}}\right)^2, \quad (3.19)$$

with [6, 7, 27]

$$\begin{aligned} \delta_{\text{PS}}^{(1)} &= \frac{73}{4} - \frac{7}{6}n_l + \left(\frac{11}{2} - \frac{1}{3}n_l\right) \ln \frac{\mu_{\text{R}}^2}{M_h^2}. \\ \delta_{\text{PS}}^{(2)} &= \frac{37631}{96} - \frac{363}{8}\zeta(2) - \frac{495}{8}\zeta(3) + \frac{2817}{16} \ln \frac{\mu_{\text{R}}^2}{M_h^2} + \frac{363}{16} \ln^2 \frac{\mu_{\text{R}}^2}{M_h^2} \\ &\quad + n_l \left(-\frac{7189}{144} + \frac{11}{2}\zeta(2) + \frac{5}{4}\zeta(3) - \frac{263}{12} \ln \frac{\mu_{\text{R}}^2}{M_h^2} - \frac{11}{4} \ln^2 \frac{\mu_{\text{R}}^2}{M_h^2} \right) \\ &\quad + n_l^2 \left(\frac{127}{108} - \frac{1}{6}\zeta(2) + \frac{7}{12} \ln \frac{\mu_{\text{R}}^2}{M_h^2} + \frac{1}{12} \ln^2 \frac{\mu_{\text{R}}^2}{M_h^2} \right), \end{aligned} \quad (3.20)$$

where $n_l = 5$ in our case.

$c_1^{(2)}$ is not known in the MSSM, thus only the NLO result for Γ_g^h can be calculated consistently up to now. However, along the lines of Ref. [31], one can argue that the numerical influence of $c_1^{(2)}$ is small at NNLO, and that it is justified to assume $c_1^{(2)} = c_1^{(2),\text{SM}}$ as long as this coefficient has not been computed in the MSSM. The motivation behind this procedure is two-fold: On the one hand, one reduces the dependence of the final result on the unphysical scales (this is more important for the production rate to be discussed below). On the other hand, the relative numerical influence of the coefficient $c_1^{(1)}$ through Eq. (3.19) is more important at NNLO than at NLO. Therefore, in the following we will give the numerical result for both NLO and the estimated NNLO (by setting $c_1^{(2)} = c_1^{(2),\text{SM}}$). In order to indicate that this is not the full NNLO result, we denote it by NNLO'.

Let us in the following discuss the numerical impact of $c_1^{(1)}$ to the hadronic Higgs decay rate in the two scenarios discussed in Sect. 3.1. In Fig. 5 (a) the decay rate is shown as a function of $m_{1/2}$ where the thick dotted, dashed, and solid line correspond to the LO, NLO, and NNLO' prediction for the SPS 1a scenario. For comparison, we show as thin lines the corresponding Standard Model results.

Similarly, Fig. 5 (b) shows the decay rate as a function of $m_{\tilde{t}_2}$ for the scenario of Eq. (3.8). As expected, around 850 GeV Γ_g^h is close to zero. Furthermore, one observes a screening of approximately 50% and more for $m_{\tilde{t}_2} \geq 600$ GeV. Note that according to Fig. 4 (b), it is at $m_{\tilde{t}_2} \approx 600$ GeV where M_h assumes its maximal value; the region above $m_{\tilde{t}_2} \approx 800$ GeV, on the other hand, is experimentally excluded due to the lack of a light Higgs signal at LEP.

3.3 Hadronic production rate

In the Standard Model, the total cross section as derived from the effective Lagrangian of Eq. (2.1) was shown to approximate the full result to better than 3% for $M_H < 2m_t$ if — analogous to Eq. (3.12) — the full top mass dependence at LO is factored out [9, 48]

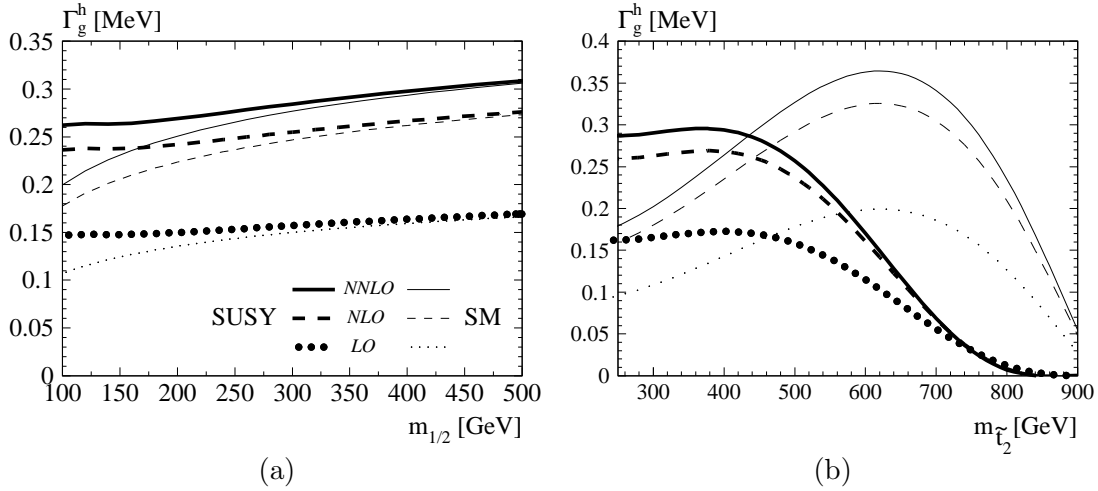


Figure 5: Hadronic decay rate for the light CP-even Higgs boson h (a) along SPS 1a, and (b) for the scenario of Eq. (3.8). The thick lines correspond to the SUSY case, the thin lines show the Standard Model results for comparison. Solid: NNLO; dashed: NLO; dotted: LO.

(see also Ref. [49]). In this case, the hadronic cross section $\sigma \equiv \sigma(pp \rightarrow h + X)$ for Higgs production can be written as

$$\begin{aligned} \sigma(z) &= \rho_0 \left(\frac{C_1}{c_1^{(0)}} \right)^2 \left[\Sigma^{(0)}(z) + \frac{\alpha_s}{\pi} \Sigma^{(1)}(z) + \left(\frac{\alpha_s}{\pi} \right)^2 \Sigma^{(2)}(z) + \dots \right] \\ &= \rho_0 \left(\frac{\alpha_s}{3\pi} \right)^2 \left[\Delta^{(0)}(z) + \frac{\alpha_s}{\pi} \Delta^{(1)}(z) + \left(\frac{\alpha_s}{\pi} \right)^2 \Delta^{(2)}(z) + \dots \right], \end{aligned} \quad (3.21)$$

where

$$\Sigma^{(n)}(z) = \sum_{i,j \in \{q, \bar{q}, g\}} \int_z^1 dx_1 \int_{z/x_1}^1 dx_2 \varphi_i(x_1) \varphi_j(x_2) \hat{\Sigma}_{ij}^{(n)} \left(\frac{z}{x_1 x_2} \right), \quad z \equiv \frac{M_h^2}{s}. \quad (3.22)$$

$\varphi_i(x)$ is the density of parton i inside the proton, M_h is the Higgs boson mass, s is the hadronic center-of-mass (c.m.) energy, and⁴

$$\rho_0 = \frac{\pi^2}{8M_h^3} F_0, \quad (3.23)$$

with F_0 from Eq. (3.13). In order to evaluate the LO, NLO, or the NNLO cross section, the second line in Eq. (3.21) has to be truncated after the term $\Delta^{(0)}$, $\Delta^{(1)}$, or $\Delta^{(2)}$, respectively. Furthermore, the parton density functions (PDFs) φ_i in Eq. (3.22) have to be used at the appropriate order.⁵ This results in different values for $\Sigma^{(n)}(z)$ and $\Delta^{(n)}(z)$, depending on the order that is being considered. The same is true for α_s which has to be set in accordance with the PDF set. Specifically, we adopt the PDF parameterizations of Ref. [52,53] where α_s is given by 0.1300, 0.1165, and 0.1153 at LO, NLO, and NNLO, respectively.

⁴Note that in Eq. (31) of Ref. [23] a factor $1/M_\phi^3$ is missing.

⁵Only approximate NNLO parton densities are currently available; with the full NNLO splitting functions being known analytically now [50,51], this shortcoming is expected to be eliminated in the near future.

Note that at this point we choose a different value for $\alpha_s(M_Z)$ as the one defined in Eq. (3.1). The latter enters the evaluation of the low energy parameters through `SoftSusy` or `SPheno`. This may be viewed as an inconsistency, but we find it more natural to have the same set of SUSY parameters at the various orders of the calculation. Besides that, the spectrum calculators — to our knowledge — do not provide control over the order of the evolution equations, and the numerical effects of the value for α_s used in Eq. (3.1) on the Higgs production cross section are small.

The LO partonic result is

$$\hat{\Sigma}_{ij}^{(0)}(x) = \delta_{ig}\delta_{jg} \delta(1-x). \quad (3.24)$$

The NLO quantity $\hat{\Sigma}_{ij}^{(1)}(x)$ can be derived from the Standard Model expression of Refs. [6,7]:

$$\begin{aligned} \hat{\Sigma}_{gg}^{(1)}(x) &= 6\zeta_2 \delta(1-x) + 12 \left[\frac{\ln(1-x)}{1-x} \right]_+ - 12x(-x+x^2+2) \ln(1-x) \\ &\quad - \frac{6(x^2+1-x)^2}{1-x} \ln(x) - \frac{11}{2}(1-x)^3, \\ \hat{\Sigma}_{qg}^{(1)}(x) &= -\frac{2}{3} (1+(1-x)^2) \ln \frac{x}{(1-x)^2} - 1 + 2x - \frac{1}{3}x^2, \\ \hat{\Sigma}_{q\bar{q}}^{(1)}(x) &= \frac{32}{27}(1-x)^3. \end{aligned} \quad (3.25)$$

The expression for $\hat{\Sigma}_{ij}^{(2)}$ is too long to be quoted here. It can be extracted from Refs. [13–15]. In analogy to the discussion below Eq. (3.20), we define an approximate NNLO result by setting $c_1^{(2)} = c_1^{(2),\text{SM}}$ and denote it by NNLO’.

For convenience, we explicitly give the relation between the $\Delta^{(n)}$ and the $\Sigma^{(n)}$, $n = 0, 1, 2$:

$$\begin{aligned} \Delta^{(0)} &= \Sigma^{(0)}, \quad \Delta^{(1)} = \Sigma^{(1)} + 2 \frac{c_1^{(1)}}{c_1^{(0)}} \Sigma^{(0)}, \\ \Delta^{(2)} &= \Sigma^{(2)} + 2 \frac{c_1^{(1)}}{c_1^{(0)}} \Sigma^{(1)} + \left[\left(\frac{c_1^{(1)}}{c_1^{(0)}} \right)^2 + 2 \frac{c_1^{(2)}}{c_1^{(0)}} \right] \Sigma^{(0)}. \end{aligned} \quad (3.26)$$

The quantities $\Sigma^{(n)}$ are independent of the specific model under consideration. A publicly available numerical program for their evaluation is in preparation [54].

For illustration of the numerical effects on the total Higgs production cross section in gluon fusion, we consider again the two exemplary cases of Sect. 3.1. The thick lines of Fig. 6 (a) show the LO (dotted), NLO (dashed), and NNLO’ (solid) cross section for the SPS1a scenario, compared to the Standard Model prediction (thin lines). At $m_{1/2} = 100$ GeV, the MSSM values are about 34% (32%) larger than the Standard Model values at NLO (NNLO’), but the difference decreases quite rapidly when $m_{1/2}$ increases. However, this difference is mostly a LO effect, as can be seen from Fig. 6 (b) which shows the NLO and the NNLO’ K-factor in the MSSM and the Standard Model. The difference of the relative corrections in both cases is less than 5%.

Fig. 7 (a), on the other hand, corresponds to the scenario defined in Eq. (3.8). As seen in Fig. 3 (b), C_1 vanishes for a certain value of $m_{\tilde{t}_2}$, and so does the NLO and the NNLO' cross section. Note, however, that this particular value is experimentally excluded because it corresponds to a too low Higgs mass (see Fig. 4 (b)). Nevertheless, for $m_{\tilde{t}_2} \approx 600$ GeV, where M_h is maximal, the cross section is still significantly suppressed with respect to the Standard Model. As the K-factor in SUSY tends to be a little smaller than in the Standard Model, this suppression becomes even stronger when QCD corrections are included. For example, at $m_{\tilde{t}_2} \approx 600$ GeV (or alternatively, $|X_t| \approx 900$ GeV), the ratio $\sigma^{\text{MSSM}}/\sigma^{\text{SM}}$ is 0.58 at LO, 0.52 at NLO, and 0.48 at NNLO'.

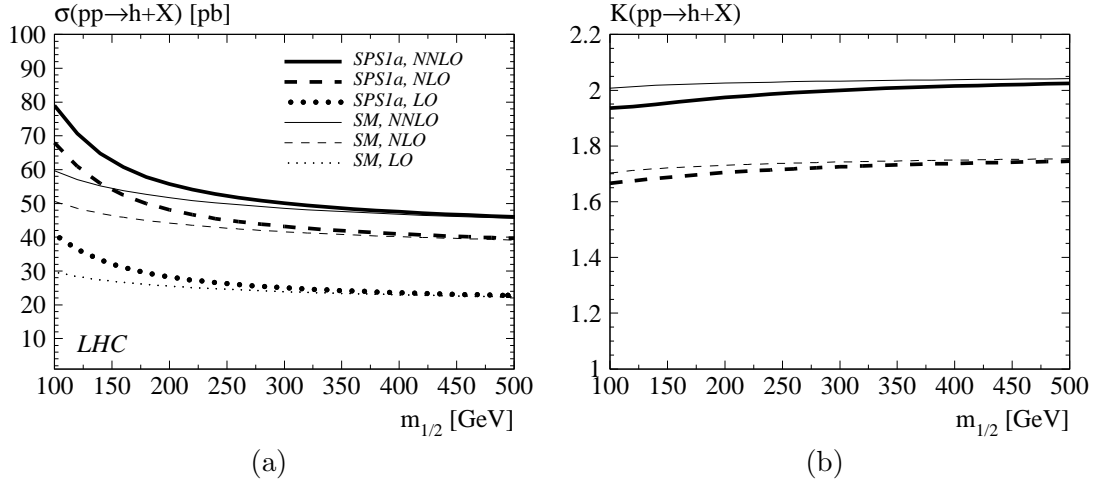


Figure 6: (a) Total cross section at LO (dotted), NLO (dashed), and NNLO' (solid) along the slope of SPS 1a (thick lines). For comparison, also the Standard Model result is shown (thin lines). It depends on $m_{1/2}$ due to the variation of M_h with this parameter. (b) NLO and NNLO' K-factor for the SPS 1a scenario (thick lines) and for the Standard Model (thin lines).

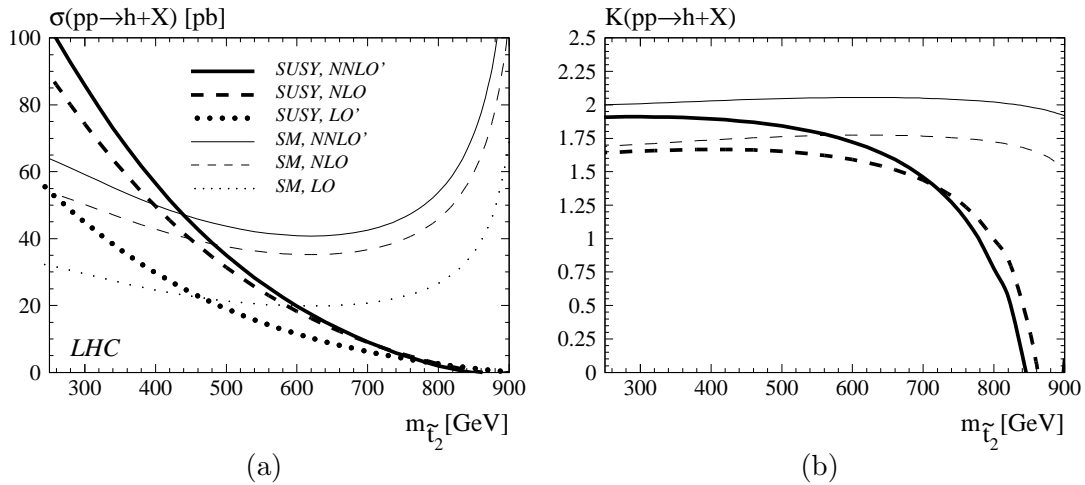


Figure 7: (a) Cross section and (b) K-factor for the scenario defined in Eq. (3.8) (thick lines) and for the Standard Model (thin lines). Dotted lines correspond to LO, dashed lines to NLO, and solid lines to NNLO'.

3.4 Discussion

In a model where the gluon-Higgs coupling is mediated predominantly by heavy particles, it had already been observed that the radiative corrections to the hadronic production and decay processes are not very sensitive to the specifics of this coupling [31, 55]. This is due to the fact that the radiative corrections are dominated by soft gluon effects which do not resolve the gluon-Higgs vertex [11–13, 56].⁶

Aside from this, for typical MSSM benchmark points, even the Wilson coefficient of the effective gluon-Higgs coupling itself is numerically rather close to its Standard Model value, both at LO and NLO. Only if at least one of the scalar top quarks is relatively light ($m_{\tilde{t}} \lesssim 400$ GeV), a significant deviation from the Standard Model result is observed. This is because the stop Yukawa coupling is proportional to m_t^2 rather than $m_{\tilde{t}}^2$. In combination with the loop amplitude of Fig. 1 (b),(c), this leads to a suppression factor $m_t^2/m_{\tilde{t}}^2$. In contrast to this, for the top quark contribution there is a cancellation between the Yukawa coupling $\sim m_t$ and a factor $1/m_t$ from the loop amplitude.

We pointed out that this suppression of the squark contribution may be compensated by a large absolute value of the parameter $X_t = A_t - \mu_{\text{SUSY}} \cot \beta$. According to Eq. (2.9), this corresponds to a stop mixing angle of the order of $\theta_t = \pi/4$, and a large mass splitting between $m_{\tilde{t}_1}$ and $m_{\tilde{t}_2}$. However, the value of X_t is crucial for the exact value of the light Higgs boson mass M_h . This restricts $|X_t|$ to less than about 3 TeV. In Eq. (3.8), we have chosen a set of low energy parameters which fulfills this condition, but where the Wilson coefficient C_1 for the gluon-Higgs interaction is very different from its Standard Model value (see Fig. 3 (b)) and leads to a strongly reduced production and decay rate. Since also here the QCD corrections tend to be smaller than in the Standard Model, this cancellation effect of top and stop contributions is even stronger when QCD corrections are included.

4. Conclusions

We have analytically calculated the NLO QCD contribution to the effective gluon-Higgs coupling in the MSSM due to the scalar partners of the top quark. Scalar bottom effects are generally suppressed by $m_b^2/m_{\tilde{b}}^2$ or $m_b \mu_{\text{SUSY}}/m_{\tilde{b}}^2$ and have been neglected. The calculation involves Feynman diagrams with three massive particles (gluino, top quark, stop quark) which leads to very long analytic expressions for the final result. Therefore, we make it available in the form of a `Fortran` routine, described in App. C.

The results for the effective coupling were used to evaluate the hadronic Higgs decay rate and the production cross section through NLO in QCD, and to derive a NNLO estimate of these quantities. The QCD corrections in the MSSM tend to be a bit smaller than in the Standard Model. However, this effect is in general below 5%. In regions of the

⁶It is remarkable, however, that the resummation of these soft-gluon effects gives only an effect of about 6% [56] with respect to the fixed order NNLO result. This is usually interpreted as a sign of the stability of the NNLO prediction.

MSSM parameter space where the Higgs coupling to gluons is particularly small due to a cancellation between the quark and the squark contribution, the reduced K-factor amplifies this effect. Nevertheless, even here the K-factor in the Standard Model provides a fairly accurate approximation to the MSSM value.

We conclude by noting that the methods of our calculation should be immediately applicable to the photonic production and decay rate of an MSSM Higgs boson, as well as to pseudo-scalar Higgs production. Inclusion of sbottom effects is also possible, but requires a careful treatment of the bottom threshold in the Feynman diagrams.

Acknowledgments. The authors are grateful to M. Faisst, S. Heinemeyer, and S. Kraml for useful discussions. RVH is supported by *Deutsche Forschungsgemeinschaft*, contract HA 2990/2-1.

A. Feynman rules

In this appendix, we collect the Feynman rules that have been used in our calculation of the NLO coefficient function C_1 . The notation follows closely Ref. [57].

A.1 Definitions

In the following, p , k , and p_n ($n = 1, 2, 3$) denote incoming four-momenta; the various indices have the following meaning:

$$\begin{aligned}
 r, s, t, u & : \text{color triplet indices} \\
 a, b, c & : \text{color octet indices} \\
 \mu, \nu, \rho & : \text{Lorentz indices} \\
 i, j, k, l & : \text{squark mass eigenstate indices} \\
 A, B & : \text{flavor indices}
 \end{aligned}$$

Furthermore, we introduce

$$\begin{aligned}
 [T^a, T^b] &= if^{abc}T^c, \quad \{T^a, T^b\} = \frac{1}{n_c}\delta^{ab} + d^{abc}T^c, \\
 P_L &= \frac{1 - \gamma_5}{2}, \quad P_R = \frac{1 + \gamma_5}{2}, \\
 \mathcal{R}^q &= \begin{pmatrix} \mathcal{R}_{11}^q & \mathcal{R}_{12}^q \\ \mathcal{R}_{21}^q & \mathcal{R}_{22}^q \end{pmatrix} = \begin{pmatrix} \cos \theta_q & \sin \theta_q \\ -\sin \theta_q & \cos \theta_q \end{pmatrix}, \\
 \mathcal{S}^q &= \begin{pmatrix} \mathcal{S}_{11}^q & \mathcal{S}_{12}^q \\ \mathcal{S}_{21}^q & \mathcal{S}_{22}^q \end{pmatrix} = \begin{pmatrix} \cos 2\theta_q & -\sin 2\theta_q \\ -\sin 2\theta_q & -\cos 2\theta_q \end{pmatrix}.
 \end{aligned} \tag{A.1}$$

$\theta_q \in [0, \frac{\pi}{2})$ is the squark mixing angle defined through

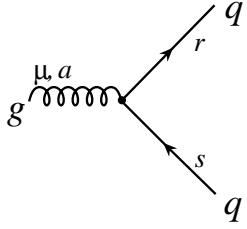
$$\sin 2\theta_q = \frac{2m_q a_q}{m_{\tilde{q}_1}^2 - m_{\tilde{q}_2}^2}, \quad \cos 2\theta_q = \frac{m_{\tilde{q}_L}^2 - m_{\tilde{q}_R}^2}{m_{\tilde{q}_1}^2 - m_{\tilde{q}_2}^2}, \tag{A.2}$$

where, by definition, we assume $m_{\tilde{q}_1} \leq m_{\tilde{q}_2}$, and

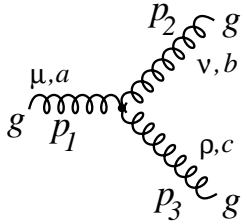
$$X_q = A_q - \mu_{\text{SUSY}} \cdot \begin{cases} \cot \beta, & \text{for } q \in \{u, c, t\} \\ \tan \beta, & \text{for } q \in \{d, s, b\} \end{cases}. \tag{A.3}$$

A_q and μ_{SUSY} are soft SUSY breaking parameters (see Ref. [34], for example).

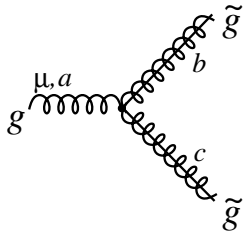
A.2 Feynman rules used in this calculation



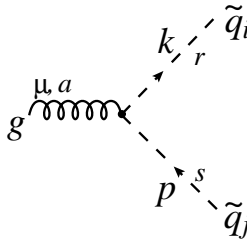
$$ig_s T_{rs}^a \gamma^\mu$$



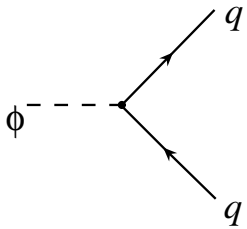
$$g_s f^{abc} [(p_1 - p_2)^\rho g^{\mu\nu} + (p_2 - p_3)^\mu g^{\nu\rho} + (p_3 - p_1)^\nu g^{\mu\rho}]$$



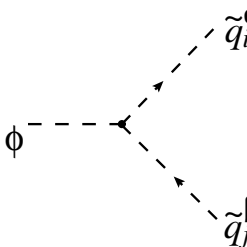
$$g_s f^{abc} \gamma^\mu$$



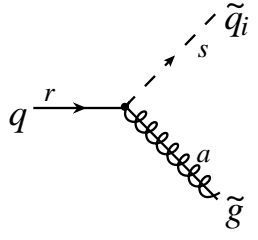
$$ig_s T_{rs}^a (p - k)^\mu \delta_{ij}$$



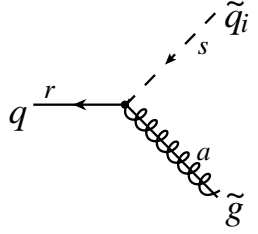
$$i \frac{m_q}{v} g_q^\phi$$



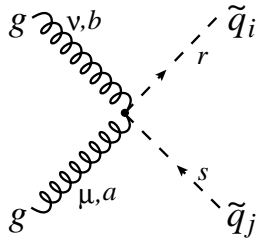
$$i \frac{m_q^2}{v} g_{q,ij}^\phi$$



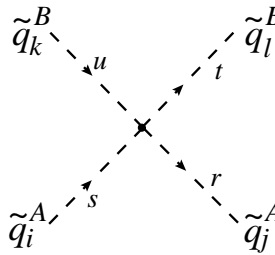
$$ig_s T_{rs}^a \sqrt{2} (\mathcal{R}_{i1}^q P_L - \mathcal{R}_{i2}^q P_R)$$



$$ig_s T_{rs}^a \sqrt{2} (\mathcal{R}_{i1}^q P_R - \mathcal{R}_{i2}^q P_L)$$



$$-ig_s^2 \left(\frac{1}{3} \delta_{ab} \delta_{rs} + d_{abc} T_{rs}^c \right) g_{\mu\nu} \delta_{ij}$$



$$ig_s^2 \left[T_{rs}^a T_{tu}^a \mathcal{S}_{ij}^A \mathcal{S}_{kl}^B + T_{ru}^a T_{ts}^a \mathcal{S}_{il}^A \mathcal{S}_{kj}^A \delta_{AB} \right], \quad (\mathcal{S}^A \equiv \mathcal{S}^{q^A})$$

We only give the values for the couplings to the light Higgs here; the couplings to the heavy Higgs can be obtained from the latter through the replacement $\alpha \rightarrow \alpha + \pi/2$. The top-Higgs coupling is

$$g_t^h = \frac{\cos \alpha}{\sin \beta}, \quad (\text{A.4})$$

and the stop-Higgs couplings are

$$g_{t,ij}^\phi = g_{t,ij}^{\phi, \text{EW}} + g_{t,ij}^{\phi, \mu} + g_{t,ij}^{\phi, \alpha}, \quad (\text{A.5})$$

with

$$\begin{aligned}
g_{t,11}^{h,\text{EW}} &= c_1^{\text{EW}} \cos^2 \theta_t + c_2^{\text{EW}} \sin^2 \theta_t, \\
g_{t,22}^{h,\text{EW}} &= c_1^{\text{EW}} \sin^2 \theta_t + c_2^{\text{EW}} \cos^2 \theta_t, \\
g_{t,12}^{h,\text{EW}} &= g_{t,21}^{h,\text{EW}} = \frac{1}{2}(c_2^{\text{EW}} - c_1^{\text{EW}}) \sin 2\theta_t, \\
g_{t,11}^{h,\mu} &= -g_{t,22}^{h,\mu} = \frac{\mu_{\text{SUSY}}}{m_t} \frac{\cos(\alpha - \beta)}{\sin^2 \beta} \sin 2\theta_t, \\
g_{t,12}^{h,\mu} &= g_{t,21}^{h,\mu} = \frac{\mu_{\text{SUSY}}}{m_t} \frac{\cos(\alpha - \beta)}{\sin^2 \beta} \cos 2\theta_t, \\
g_{t,11}^{h,\alpha} &= \frac{\cos \alpha}{\sin \beta} \left[2 + \frac{m_{\tilde{t}_1}^2 - m_{\tilde{t}_2}^2}{2m_t^2} \sin^2 2\theta_t \right], \\
g_{t,22}^{h,\alpha} &= \frac{\cos \alpha}{\sin \beta} \left[2 - \frac{m_{\tilde{t}_1}^2 - m_{\tilde{t}_2}^2}{2m_t^2} \sin^2 2\theta_t \right], \\
g_{t,12}^{h,\alpha} &= g_{t,21}^{h,\alpha} = \frac{\cos \alpha}{\sin \beta} \frac{m_{\tilde{t}_1}^2 - m_{\tilde{t}_2}^2}{2m_t^2} \sin 2\theta_t \cos 2\theta_t,
\end{aligned} \tag{A.6}$$

where

$$\begin{aligned}
c_1^{\text{EW}} &= -\frac{M_Z^2}{m_t^2} \left(1 - \frac{4}{3} \sin^2 \theta_W \right) \sin(\alpha + \beta) \\
c_2^{\text{EW}} &= -\frac{M_Z^2}{m_t^2} \frac{4}{3} \sin^2 \theta_W \sin(\alpha + \beta), \\
\sin \theta_W &= \sqrt{1 - \frac{M_W^2}{M_Z^2}},
\end{aligned} \tag{A.7}$$

and

$$v = \frac{2M_W}{g} = \frac{1}{\sqrt{\sqrt{2}G_{\text{F}}}} = \sqrt{v_1^2 + v_2^2} \approx 246 \text{ GeV}, \tag{A.8}$$

with v_1, v_2 the vacuum expectation values of the two Higgs doublets. In Eq.(A.6) we have already expressed the trilinear couplings of the soft SUSY breaking terms through independent parameters:

$$A_t = \frac{m_{\tilde{t}_1}^2 - m_{\tilde{t}_2}^2}{2m_t} \sin 2\theta_t + \mu_{\text{SUSY}} \cot \beta. \tag{A.9}$$

The electroweak radiative corrections to this formula need not be considered here.

B. Renormalization and decoupling constants

In order to arrive at a finite NLO result, the parameters appearing in the LO coefficient function given in Eq.(2.8) have to be renormalized. This includes the strong coupling

constant α_s , the top quark mass m_t , the top squark masses $m_{\tilde{t}_i}$, and the mixing angle θ_t , whereas the angles α , β and θ_W are not renormalized, because we consider QCD corrections only.

First, the top quark and the SUSY partners are decoupled from the bare coupling constant through the relation

$$\alpha_s^{\text{B}} = (\zeta_g^{\text{B}})^2 \tilde{\alpha}_s^{\text{B}}, \quad (\text{B.1})$$

where $\tilde{\alpha}_s^{\text{B}}$ and α_s^{B} denote the bare couplings in the full theory and in five-flavor QCD, respectively. In the $\overline{\text{DR}}$ scheme, we find

$$(\zeta_g^{\text{B}})^2 = 1 - \frac{\alpha_s}{\pi} \left(\frac{1}{\epsilon} \left[\frac{1}{6} C_A + \frac{1}{2} T \right] + L(\epsilon) \right) + \mathcal{O}(\alpha_s^2), \quad (\text{B.2})$$

where $C_A = 3$, $T = 1/2$ and

$$\begin{aligned} L(\epsilon) &= \frac{1}{12} [2C_A L_{\tilde{g}} + T(L_{\tilde{t}_1} + L_{\tilde{t}_2} + 4L_t)] \\ &\quad + \frac{\epsilon}{12} \left[C_A L_{\tilde{g}}^2 + \frac{1}{2} T (L_{\tilde{t}_1}^2 + L_{\tilde{t}_2}^2) + 2T L_t^2 + (C_A + 3T) \zeta_2 \right], \quad (\text{B.3}) \\ L_t &= \ln \frac{\mu_{\text{R}}^2}{m_t^2}, \quad L_{\tilde{t}_i} = \ln \frac{\mu_{\text{R}}^2}{m_{\tilde{t}_i}^2}, \quad L_{\tilde{g}} = \ln \frac{\mu_{\text{R}}^2}{m_{\tilde{g}}^2}. \end{aligned}$$

α_s^{B} is then renormalized through

$$\frac{\alpha_s^{\text{B}}}{\alpha_s^{\overline{\text{DR}}}} = 1 + \frac{\alpha_s}{\pi} \frac{1}{\epsilon} \left[-\frac{11}{12} C_A + \frac{1}{3} T n_l \right], \quad (\text{B.4})$$

where $\alpha_s^{\overline{\text{DR}}}$ denotes the $\overline{\text{DR}}$ expression for the strong coupling constant in QCD with $n_l = 5$ active flavors. We will comment on the transformation to the more familiar $\overline{\text{MS}}$ scheme below.

For the quark and squark masses, we adopt the on-shell scheme, where they are defined as the real part of the pole of the corresponding propagator. Furthermore, we define the renormalized squark mixing angle by requiring that the non-diagonal two-point function $\langle \tilde{t}_1 \tilde{t}_2 \rangle$ vanishes at a certain momentum transfer q_0 ; i.e., the two squarks propagate independently from each other at the scale q_0 . In practice, q_0 is chosen to be of the order of the squark masses. The counter terms can be found in Ref. [58], for example. For convenience, we list them explicitly in our notation.

In DRED, the relation between the bare and the pole top quark mass reads

$$\begin{aligned} \frac{m_t^{\text{B}}}{m_t} &= 1 + C_F \frac{\alpha_s}{\pi} \left\{ -\frac{1}{2\epsilon} - \frac{5}{4} - \frac{3}{4} L_t - \frac{m_{\tilde{g}}^2}{4m_t^2} (1 + L_{\tilde{g}}) + \sum_{i=1}^2 \left[\frac{m_{\tilde{t}_i}^2}{8m_t^2} (1 + L_{\tilde{t}_i}) \right. \right. \\ &\quad \left. \left. + \frac{1}{8} \left(1 + \frac{m_{\tilde{g}}^2}{m_t^2} - \frac{m_{\tilde{t}_i}^2}{m_t^2} + 2(-1)^i \frac{m_{\tilde{g}}}{m_t} \sin 2\theta_t \right) B_0^{\text{fin}}(m_t^2, m_{\tilde{g}}, m_{\tilde{t}_i}) \right] \right\}, \quad (\text{B.5}) \end{aligned}$$

where $C_F = 4/3$. The only difference between DRED and Dimensional Regularization (DREG) comes from the gluon-exchange diagram which changes the constant “5/4” into “1” in the case of DREG. The relation for the top squark mass $m_{\tilde{t}_1}$ is given by

$$\begin{aligned} \frac{m_{\tilde{t}_1}^{\text{B}}}{m_{\tilde{t}_1}} = 1 + C_F \frac{\alpha_s}{\pi} \left\{ \frac{1}{8m_{\tilde{t}_1}^2 \epsilon} \left[4m_{\tilde{g}}m_t \sin 2\theta_t - 4m_{\tilde{g}}^2 - 4m_t^2 + (m_{\tilde{t}_2}^2 - m_{\tilde{t}_1}^2) \sin^2 2\theta_t \right] \right. \\ - \frac{3}{4} - \frac{\sin^2 2\theta_t}{8} - \left(\frac{1}{4} + \frac{\sin^2 2\theta_t}{8} \right) L_{\tilde{t}_1} - \frac{m_{\tilde{g}}^2}{4m_{\tilde{t}_1}^2} (1 + L_{\tilde{g}}) - \frac{m_t^2}{4m_{\tilde{t}_1}^2} (1 + L_t) \\ \left. + \frac{m_{\tilde{t}_2}^2 \sin^2 2\theta_t}{8m_{\tilde{t}_1}^2} (1 + L_{\tilde{t}_2}) + \left[\frac{1}{4} + \frac{2m_{\tilde{g}}m_t \sin 2\theta_t - m_{\tilde{g}}^2 - m_t^2}{4m_{\tilde{t}_1}^2} \right] B_0^{\text{fin}}(m_{\tilde{t}_1}^2, m_t, m_{\tilde{g}}) \right\}. \end{aligned} \quad (\text{B.6})$$

The corresponding relation for the mass $m_{\tilde{t}_2}$ is obtained by interchanging the indices “1” and “2” and changing the sign of $\sin 2\theta_t$.

Finally, for the mixing angle we have

$$\begin{aligned} \theta_t^{\text{B}} = \theta_t + \delta\theta_t, \\ \delta\theta_t = C_F \frac{\alpha_s}{\pi} \frac{\cos 2\theta_t}{m_{\tilde{t}_1}^2 - m_{\tilde{t}_2}^2} \left\{ \frac{4m_{\tilde{g}}m_t + (m_{\tilde{t}_2}^2 - m_{\tilde{t}_1}^2) \sin 2\theta_t}{4\epsilon} \right. \\ \left. + \frac{\sin 2\theta_t}{4} \left[m_{\tilde{t}_2}^2 (1 + L_{\tilde{t}_2}) - m_{\tilde{t}_1}^2 (1 + L_{\tilde{t}_1}) \right] + m_{\tilde{g}}m_t B_0^{\text{fin}}(q_0^2, m_t, m_{\tilde{g}}) \right\}. \end{aligned} \quad (\text{B.7})$$

For $q^2 \leq (m_1 - m_2)^2$, $B_0^{\text{fin}}(q^2, m_1, m_2)$ is given by

$$B_0^{\text{fin}}(q^2, m_1, m_2) = 2 - \ln \frac{m_1 m_2}{\mu_{\text{R}}^2} + \frac{m_1^2 - m_2^2}{q^2} \ln \frac{m_2}{m_1} + \frac{M_+ M_-}{q^2} \ln \frac{M_+ + M_-}{M_+ - M_-}, \quad (\text{B.8})$$

with $M_{\pm} = \sqrt{(m_1 \pm m_2)^2 - q^2}$. The analytical expressions for the other kinematical regions can be derived from this expression by proper analytical continuation. Note that the counter terms in the $\overline{\text{DR}}$ scheme are obtained by discarding the finite parts at order α_s .

The decoupling constant entering Eq. (2.6) is defined in analogy to Eq. (B.1) via the relation of the bare gluon field of the full theory, $\tilde{G}_{\mu}^{\text{B}}$, (i.e. including the top quark and the SUSY particles) and the effective theory, G_{μ}^{B} :

$$G_{\mu}^{\text{B}} = \sqrt{\zeta_3^{\text{B}}} \tilde{G}_{\mu}^{\text{B}}, \quad (\text{B.9})$$

where

$$\zeta_3^{\text{B}} = 1 + \frac{\alpha_s}{\pi} \left[\frac{1}{\epsilon} \left(\frac{1}{6} C_A + \frac{1}{2} T \right) + L(\epsilon) \right] + \mathcal{O}(\alpha_s^2), \quad (\text{B.10})$$

with $L(\epsilon)$ from Eq. (B.3).

$\alpha_s^{\overline{\text{DR}}}$ is transformed from the $\overline{\text{DR}}$ to the $\overline{\text{MS}}$ scheme through a finite shift [59]; however, we found that this shift is canceled by a finite shift in the decoupling constant ζ_g^{B} and

the operator renormalization Z_{11} , given in Eq.(2.2). Our final result is thus expressed in terms of the $\overline{\text{MS}}$ coupling α_s for standard five-flavor QCD, on-shell quark and squark masses, and the squark mixing angle as defined in Eq.(B.7) (the gluino mass is unaffected by renormalization at the order considered here).

C. Description of evalcsusy.f

In this Appendix we give details on the usage of the Fortran program `evalcsusy.f` [38]. The distribution includes the files

```
evalcsusy.f  common-slha.f  functions.f  readslha.f  slhablocks.f
```

as well as the Fortran code for the two-loop results of C_1 as defined in Eq.(2.5); the latter is contained in the directory `obj/`. For compilation one also needs the CERN libraries `kernlib` and `mathlib`.

In a first step, object files are generated with

```
> f77 -c functions.f readslha.f slhablocks.f obj/*.f
```

The executable is then obtained by saying

```
> f77 -o evalcsusy evalcsusy.f functions.o readslha.o \
  slhablocks.o obj/*.o -L'cernlib -v pro kernlib,mathlib'
```

`evalcsusy` is invoked as

```
> ./evalcsusy <infile> <outfile>
```

where `<infile>` and `<outfile>` are the in- and output file, respectively. Both files obey the SUSY Les Houches accord (SLHA) [39] which makes it straightforward to interface `evalcsusy.f` with a spectrum calculator. The basic idea of the SLHA is to group the parameters into various blocks which have a uniquely defined structure in order to ensure universality. For our process we need some parameters (the precise specification can be seen in the example presented below) of the blocks `SMINPUTS`, `MASS`, `ALPHA`, `HMIX`, `STOPMIX` and `MINPAR`. In addition, we introduce a new block `CREIN` specific to `evalcsusy.f`, where the ratio μ_R/M_h and the parameter q_0 is defined (see Eq.(3.2) and Sect.B). The latter is actually composed out of the three quantities q_0^c , q_{01} and q_{02} via the relation

$$q_0 = q_0^c + q_{01}m_{\tilde{t}_1} + q_{02}m_{\tilde{t}_2}. \quad (\text{C.1})$$

If q_{01} (q_{02}) is not defined, its value is set to zero.

`evalcsusy.f` copies the contents of the input file to the output file and appends an additional block `HGGSUSY`. Its structure is as follows:

Block HGGUSUSY

```
101 :  $c_1^{(0),SM}$ 
102 :  $c_1^{(1),SM}$ 
103 :  $c_1^{(2),SM}$ 
201 :  $c_1^{(0)}$ 
202 :  $c_1^{(1)}$ 
1001 :  $g_t^h$ 
1011 :  $g_{t,11}^h$ 
1022 :  $g_{t,22}^h$ 
1012 :  $g_{t,12}^h$ 
1021 :  $g_{t,21}^h$ 
```

It contains the results for the one- and two-loop coefficients (c.f. Eq. (2.5)) both for the Standard Model ($c_1^{(0),SM}$ and $c_1^{(1),SM}$) and the MSSM ($c_1^{(0)}$ and $c_1^{(1)}$). Furthermore, the three-loop Standard Model term is given. In addition, it provides numerical values for the top and stop Yukawa couplings g_t^h and $g_{t,ij}^h$ (see Eqs. (A.4)–(A.6)).

Let us exemplify the use of `evalcsusy.f` by considering the SPS 1a point given in Eq. (3.3). Defining in addition the Standard Model parameters of Eq. (3.1) in the block `SMINPUTS`, the output of `SoftSusy` [42] looks as follows (after adding the block `CREIN`):

Block CREIN

```
6  0.d0      # q0c
61 .5d0      # q01
62 .5d0      # q02
7  1.d0      # renormalization scale muR/mh
```

Block SMINPUTS # Standard Model inputs

```
3  1.18000000e-01 # alpha_s(MZ)MSbar
4  9.11876000e+01 # MZ(pole)
6  1.78000000e+02 # Mtop(pole)
```

Block MINPAR # SUSY breaking input parameters

```
3  1.00000000e+01 # tanb
4  1.00000000e+00 # sign(mu)
1  1.00000000e+02 # m0
2  2.50000000e+02 # m12
5  -1.00000000e+02 # A0
```

Block MASS # Mass spectrum

```
#PDG code      mass      particle
```

```

        24      8.02591534e+01   # MW
        25      1.12153306e+02   # h0
1000006      3.97398225e+02   # ~t_1
1000021      6.11147741e+02   # ~g
2000006      5.86830420e+02   # ~t_2

Block alpha   # Effective Higgs mixing parameter
        -1.13348399e-01   # alpha

Block hmix Q= 4.661391312e+02 # Higgs mixing parameters
        1      3.65690378e+02 # mu

Block stopmix # stop mixing matrix
  1  1      5.34006091e-01   # O_{11}
  1  2      8.45480617e-01   # O_{12}

```

where only those parameters are displayed which are needed in `evalcsusy.f`. Using this file as input for `evalcsusy.f`, its contents are copied to the output file, and the block

```

Block HGG SUSY
  101      0.10000000E+01   #          cSM 1-loop
  102      0.27500000E+01   #          cSM 2-loop
  103      0.35160026E+01   #          cSM 3-loop
  201      0.10343231E+01   #          cSUSY 1-loop
  202      0.24377938E+01   #          cSUSY 2-loop
1001      0.99853850E+00   #          gth
1011     -0.53035841E+00   #          gth11
1022      0.42680033E+01   #          gth22
1012      0.11983135E+01   #          gth12
1021      0.11983135E+01   #          gth21

```

is added.

References

- [1] T. Han and S. Willenbrock, *QCD correction to the $pp \rightarrow WH$ and ZH total cross-sections*, Phys. Lett. **B 273**, 167 (1991)
- [2] T. Figy, C. Oleari, D. Zeppenfeld, *Next-to-leading order jet distributions for Higgs boson production via weak-boson fusion*, Phys. Rev. **D 68**, 073005 (2003)
- [3] W. Beenakker, S. Dittmaier, M. Krämer, B. Plümper, M. Spira, P.M. Zerwas, *Higgs radiation off top quarks at the Tevatron and the LHC*, Phys. Rev. Lett. **87**, 201805 (2001)
- [4] S. Dawson, L.H. Orr, L. Reina, D. Wackerroth, *Associated top quark Higgs boson production at the LHC*, Phys. Rev. **D 67**, 071503 (2003)

- [5] S. Dawson, C. Jackson, L.H. Orr, L. Reina, D. Wackerroth, *Associated Higgs production with top quarks at the Large Hadron Collider: NLO QCD corrections*, Phys. Rev. **D 68**, 034022 (2003)
- [6] S. Dawson, *Radiative corrections to Higgs boson production*, Nucl. Phys. **B 359**, 283 (1991)
- [7] A. Djouadi, M. Spira, P.M. Zerwas, *Production of Higgs bosons in proton colliders: QCD corrections*, Phys. Lett. **B 264**, 440 (1991)
- [8] D. Graudenz, M. Spira, P.M. Zerwas, *QCD corrections to Higgs boson production at proton-proton colliders*, Phys. Rev. Lett. **70**, 1372 (1993)
- [9] M. Spira, A. Djouadi, D. Graudenz, P.M. Zerwas, *Higgs boson production at the LHC*, Nucl. Phys. **B 453**, 17 (1995)
- [10] R.V. Harlander, *Virtual corrections to $gg \rightarrow H$ to two loops in the heavy top limit*, Phys. Lett. **B 492**, 74 (2000)
- [11] R.V. Harlander and W.B. Kilgore, *Soft and virtual corrections to $pp \rightarrow H + X$ at NNLO*, Phys. Rev. **D 64**, 01301 (2001)
- [12] S. Catani, D. de Florian, M. Grazzini, *Higgs production in hadron collisions: Soft and virtual QCD corrections at NNLO*, JHEP **0105**, 025 (2001)
- [13] R.V. Harlander and W.B. Kilgore, *Next-to-next-to-leading order Higgs production at hadron colliders*, Phys. Rev. Lett. **88**, 201801 (2002)
- [14] C. Anastasiou and K. Melnikov, *Higgs boson production at hadron colliders in NNLO QCD*, Nucl. Phys. **B 646**, 220 (2002)
- [15] V. Ravindran, J. Smith, W.L. van Neerven, *NNLO corrections to the total cross section for Higgs boson production in hadron hadron collisions*, Nucl. Phys. **B 665**, 325 (2003)
- [16] O. Brein, A. Djouadi, R. Harlander, *NNLO QCD corrections to the Higgs-strahlung processes at hadron colliders*, Phys. Lett. **B 579**, 149 (2004)
- [17] M.L. Ciccolini, S. Dittmaier, M. Krämer, *Electroweak radiative corrections to associated $W H$ and $Z H$ production at hadron colliders*, Phys. Rev. **D 68**, 073003 (2003)
- [18] O. Brein, *et al.*, *Precision calculations for associated $W H$ and $Z H$ production at hadron colliders*, hep-ph/0402003, in: K.A. Assamagan *et al.*, hep-ph/0406152
- [19] U. Aglietti, R. Bonciani, G. Degrossi, A. Vicini, *Two-loop light fermion contribution to Higgs production and decays*, hep-ph/0404071
- [20] G. Degrossi and F. Maltoni, *Two-loop electroweak corrections to Higgs production at hadron colliders*, hep-ph/0407249
- [21] A. Djouadi and P. Gambino, *Leading electroweak correction to Higgs boson production at proton colliders*, Phys. Rev. Lett. **73**, 2528 (1994)
- [22] M. Steinhauser, *Higgs decay into gluons up to $\mathcal{O}(\alpha_s^3 G_F m_t^2)$* , Phys. Rev. **D 59**, 054005 (1999)
- [23] R.V. Harlander and M. Steinhauser, *Hadronic Higgs Production and Decay in Supersymmetry at Next-to-Leading Order*, Phys. Lett. **B 574**, 258-268 (2003)
- [24] B.C. Allanach *et al.*, *The Snowmass points and slopes: Benchmarks for SUSY searches*, in *Proc. of the APS/DPF/DPB Summer Study on the Future of Particle Physics (Snowmass 2001)* ed. N. Graf, Eur. Phys. J. **C 25**, 113 (2002), [eConf **C010630** (2001) P125]

- [25] M. Carena, S. Heinemeyer, C.E.M. Wagner, G. Weiglein, *Suggestions for improved benchmark scenarios for Higgs-boson searches at LEP2*, hep-ph/9912223
- [26] A. Djouadi, *Squark effects on Higgs boson production and decay at the LHC*, Phys. Lett. **B 435**, 101 (1998)
- [27] K.G. Chetyrkin, B.A. Kniehl, M. Steinhauser, *Hadronic Higgs decay to order α_s^4* , Phys. Rev. Lett. **79**, 353 (1997)
- [28] M. Krämer, E. Laenen, M. Spira, *Soft gluon radiation in Higgs boson production at the LHC*, Nucl. Phys. **B 511**, 523 (1998)
- [29] K.G. Chetyrkin, B.A. Kniehl, M. Steinhauser, *Decoupling relations to $\mathcal{O}(\alpha_s^3)$ and their connection to low-energy theorems*, Nucl. Phys. **B 510**, 61 (1998)
- [30] V.P. Spiridonov, *Anomalous dimension of $G_{\mu\nu}^2$ and β -function*, IYaI-P-0378 (1984)
- [31] R.V. Harlander and M. Steinhauser, *Effects of SUSY-QCD in hadronic Higgs production at next-to-next-to-leading order*, Phys. Rev. **D 68**, 111701 (2003)
- [32] M. Steinhauser, *Results and techniques of multi-loop calculations*, Phys. Reports **364**, 247 (2002)
- [33] A.I. Davydychev and J.B. Tausk, *Two loop selfenergy diagrams with different masses and the momentum expansion*, Nucl. Phys. **B 397**, 123 (1993)
- [34] S.P. Martin, *A supersymmetry primer*, in: G.L. Kane (ed.): *Perspectives on supersymmetry*, 1-98; hep-ph/9709356
- [35] I. Jack, D.R.T. Jones, S.P. Martin, M.T. Vaughn, Y. Yamada, *Decoupling of the epsilon scalar mass in softly broken supersymmetry*, Phys. Rev. **D 50**, 5481 (1994)
- [36] I. Jack and D.R.T. Jones, *Regularisation of supersymmetric theories*, hep-ph/9707278
- [37] J.A. Vermaseren, *New features of FORM*, math-ph/0010025
- [38] The source code can be obtained from the URL
<http://www-ttp.physik.uni-karlsruhe.de/Progdata/ttp04/ttp04-19/>
- [39] P. Skands *et al.*, *SUSY Les Houches accord: Interfacing SUSY spectrum calculators, decay packages, and event generators*, hep-ph/0311123
- [40] T. Seidensticker, *Automatic application of successive asymptotic expansions of Feynman diagrams*, hep-ph/9905298;
R. Harlander, T. Seidensticker, M. Steinhauser, *Corrections of $\mathcal{O}(\alpha_s)$ to the decay of the Z boson into bottom quarks*, Phys. Lett. **B 426**, 125 (1998)
- [41] H. Baer, F.E. Paige, S.D. Protopopescu, X. Tata, *ISAJET 7.48: A Monte Carlo event generator for pp, $\bar{p}p$, and e^+e^- reactions*, hep-ph/0001086
- [42] B.C. Allanach, *SOFTSUSY: A C++ program for calculating supersymmetric spectra*, Comp. Phys. Commun. **143**, 305 (2002)
- [43] A. Djouadi, J. L. Kneur, G. Moultaka, *SuSpect: A Fortran code for the supersymmetric and Higgs particle spectrum in the MSSM*, hep-ph/0211331
- [44] W. Porod, *SPheno, a program for calculating supersymmetric spectra, SUSY particle decays and SUSY particle production at e^+e^- colliders*, Comp. Phys. Commun. **153**, 275 (2003)

- [45] B.C. Allanach, S. Kraml, W. Porod, *Theoretical uncertainties in sparticle mass predictions from computational tools*, JHEP **0303**, 016 (2003)
- [46] M. Carena, S. Heinemeyer, C. E. M. Wagner, G. Weiglein, *Suggestions for benchmark scenarios for MSSM Higgs boson searches at hadron colliders*, Eur. Phys. J. **C 26**, 601 (2003)
- [47] M. Carena, H.E. Haber, S. Heinemeyer, W. Hollik, C.E.M. Wagner, G. Weiglein, *Reconciling the two-loop diagrammatic and effective field theory computations of the mass of the lightest CP-even Higgs boson in the MSSM*, Nucl. Phys. **B 580**, 29 (2000)
- [48] M. Spira, *QCD effects in Higgs physics*, Fortschr. Phys. **46**, 203 (1998)
- [49] R. Harlander, *Supersymmetric Higgs production at the Large Hadron Collider*, hep-ph/0311005
- [50] S. Moch, J.A.M. Vermaseren, A. Vogt, *The three-loop splitting functions in QCD: The non-singlet case*, Nucl. Phys. **B 688**, 101 (2004)
- [51] A. Vogt, S. Moch, J.A.M. Vermaseren, *The three-loop splitting functions in QCD: The singlet case*, hep-ph/0404111
- [52] A.D. Martin, R.G. Roberts, W.J. Stirling, R.S. Thorne, *NNLO global parton analysis*, Phys. Lett. **B 531**, 216 (2002)
- [53] A.D. Martin, R.G. Roberts, W.J. Stirling, R.S. Thorne, *MRST partons and uncertainties*, hep-ph/0307262
- [54] R.V. Harlander and W.B. Kilgore, in preparation.
- [55] S. Dawson, A. Djouadi, M. Spira, *QCD Corrections to SUSY Higgs Production: The Role of Squark Loops*, Phys. Rev. Lett. **77**, 16 (1996)
- [56] S. Catani, D. de Florian, M. Grazzini, P. Nason, *Soft-gluon resummation for Higgs boson production at hadron colliders*, JHEP **0307**, 028 (2003)
- [57] S. Kraml, *Stop and sbottom phenomenology in the MSSM*, PhD thesis, Vienna University (1999), hep-ph/9903257; H. Eberl, *Strahlungskorrekturen im minimalen supersymmetrischen Standardmodell*, PhD thesis, Vienna University (1998)
- [58] A. Djouadi, P. Gambino, S. Heinemeyer, W. Hollik, C. Jünger, G. Weiglein, *Leading QCD corrections to scalar quark contributions to electroweak precision observables*, Phys. Rev. **D 57**, 4179 (1998)
- [59] S.P. Martin and M.T. Vaughn, *Regularization dependence of running couplings in softly broken supersymmetry*, Phys. Lett. **B 318**, 331 (1993)